



HAL
open science

Loss of the actin-like protein MamK has pleiotropic effects on magnetosome formation and chain assembly in *Magnetospirillum gryphiswaldense*

Emanuel Katzmann, André Scheffel, Manuela Gruska, Jürgen M Plitzko, Dirk Schüler

► To cite this version:

Emanuel Katzmann, André Scheffel, Manuela Gruska, Jürgen M Plitzko, Dirk Schüler. Loss of the actin-like protein MamK has pleiotropic effects on magnetosome formation and chain assembly in *Magnetospirillum gryphiswaldense*. *Molecular Microbiology*, 2010, 10.1111/j.1365-2958.2010.07202.x . hal-00552637

HAL Id: hal-00552637

<https://hal.science/hal-00552637>

Submitted on 6 Jan 2011

HAL is a multi-disciplinary open access archive for the deposit and dissemination of scientific research documents, whether they are published or not. The documents may come from teaching and research institutions in France or abroad, or from public or private research centers.

L'archive ouverte pluridisciplinaire **HAL**, est destinée au dépôt et à la diffusion de documents scientifiques de niveau recherche, publiés ou non, émanant des établissements d'enseignement et de recherche français ou étrangers, des laboratoires publics ou privés.

**Loss of the actin-like protein MamK has pleiotropic effects
on magnetosome formation and chain assembly in
*Magnetospirillum gryphiswaldense***

Journal:	<i>Molecular Microbiology</i>
Manuscript ID:	MMI-2010-09908.R1
Manuscript Type:	Research Article
Date Submitted by the Author:	29-Apr-2010
Complete List of Authors:	Katzmann, Emanuel; Ludwig-Maximilians-Universität München, Biologie 1, Mikrobiologie; Max Planck Institut für Biochemie, Molekulare Strukturbiologie Scheffel, André; Georgia Institute of Technology, School of Chemistry and Biochemistry Gruska, Manuela; Max Planck Institute für Biochemie, Molekulare Strukturbiologie Plitzko, Jürgen; Max Planck Institute für Biochemie, Molekulare Strukturbiologie Schüler, Dirk; Ludwig-Maximilians-Universität München, Biologie 1, Mikrobiologie
Key Words:	MamK, cytoskeleton, actin-like, magnetotactic, cryo-electron tomography

1 **Loss of the actin-like protein MamK has pleiotropic effects on magnetosome**
2 **formation and chain assembly in *Magnetospirillum gryphiswaldense***

3

4 Emanuel Katzmann^{1,2}, André Scheffel³⁼, Manuela Gruska², Jürgen M. Pitzko², Dirk
5 Schüler^{1*}

6 Email: emanuel.katzmann@bio.lmu.de, gruska@biochem.mpg.de,
7 plitzko@biochem.mpg.de

8

9 *Corresponding author

10 Telephone: +49 89 21 80 - 74502

11 Fax: +49 89 21 80 - 74515

12 Email: dirk.schueler@lmu.de

13

14 Keywords: MamK, cytoskeleton, actin-like, magnetotactic, cryo-electron tomography,
15 organelles

¹Ludwig-Maximilians-Universität München, Department Biologie I, Bereich Mikrobiologie,
Biozentrum der LMU, D-82152 Martinsried, Germany

² Max Planck Institute of Biochemistry, Department of Molecular Structural Biology, Am
Klopferspitz 18,
D-82152 Martinsried, Germany

³ Max Planck Institute for Marine Microbiology, Celsiusstr.1, D-28359 Bremen, Germany

⁼ Present address: School of Chemistry and Biochemistry, Georgia Institute of Technology,
Atlanta, GA 30332-0400, USA.

Email: ascheffel3@mail.gatech.edu

16 **Summary**

17 Magnetotactic bacteria synthesize magnetosomes, which are unique organelles
18 consisting of membrane-enclosed magnetite crystals. For magnetic orientation individual
19 magnetosome particles are assembled into well-organized chains. The actin-like MamK
20 and the acidic MamJ proteins were previously implicated in chain assembly. While
21 MamK was suggested to form magnetosome-associated cytoskeletal filaments, MamJ is
22 assumed to attach the magnetosome vesicles to these structures. Although the deletion
23 of either *mamK* in *M. magneticum*, or *mamJ* in *M. gryphiswaldense* affected chain
24 formation, the previously observed phenotypes were not fully consistent, suggesting
25 different mechanisms of magnetosome chain assembly in both organisms. Here we
26 show that in *M. gryphiswaldense* MamK is not absolutely required for chain formation.
27 Straight chains, shorter, fragmented, and ectopic, were still formed in a *mamK* deletion
28 mutant, although magnetosome filaments were absent as shown by cryo-electron
29 tomography. Loss of MamK also resulted in reduced numbers of magnetite crystals and
30 magnetosome vesicles and led to the mislocalization of MamJ. In addition, extensive
31 analysis of wildtype and mutant cells revealed previously unidentified ultrastructural
32 characteristics in *M. gryphiswaldense*. Our results suggest that, despite of their
33 functional equivalence, loss of MamK proteins in different bacteria may result in distinct
34 phenotypes, which might be due to a species-specific genetic context.

35

36 Introduction

37 The ability of magnetic navigation in magnetotactic bacteria (MTB) is based on the
38 synthesis of magnetosomes, which are complex intracellular organelles. In
39 *Magnetospirillum gryphiswaldense* MSR-1 (in the following referred to as MSR) and
40 related magnetospirilla magnetosomes comprise cubo-octahedral nanocrystals of
41 magnetite (Fe_3O_4) that are enveloped by vesicles of the magnetosome membrane (MM)
42 (Gorby *et al.*, 1988; Schüller, 2004b). Previous studies revealed that the MM is a
43 phospholipid bilayer, which is associated with a set of about 20 specific proteins (Gorby
44 *et al.*, 1988; Grünberg *et al.*, 2001; Grünberg *et al.*, 2004). In *M. magneticum* AMB-1 (in
45 the following referred to as AMB) it was shown that the MM originates via invagination
46 from the cytoplasmic membrane (CM) (Komeili *et al.*, 2006).

47 For maximum sensitivity of magnetic orientation, magnetosomes are organized within
48 single or multiple chains, which represent one of the highest structural levels found in a
49 prokaryotic cell. However, a string of magnetic dipoles has an immanent tendency of
50 collapsing to lower its magnetostatic energy unless it is properly stabilized (Kirschvink,
51 1982; Kobayashi *et al.*, 2006). Recently, it has been found that the assembly and
52 maintenance of magnetosome chains is governed by dedicated cellular structures. Two
53 complementary studies investigated chain formation in the two related magnetic bacteria
54 MSR and AMB by cryo-electron tomography (CET) (Komeili *et al.*, 2006; Scheffel *et al.*,
55 2006). CET has emerged as a powerful technology for bridging the gap between
56 protein-protein interactions and cellular architecture (Lučić *et al.*, 2005; Li and Jensen,
57 2009; Milne and Subramaniam, 2009). In CET, cells are embedded in vitreous ice in a
58 close-to-native state, thereby avoiding artifacts typically associated with conventional
59 electron microscopy. CET analysis of MSR and AMB demonstrated a cytoskeletal

60 network of filaments, 3-4 nm in diameter, which traverse the cells adjacent to the CM.
61 Magnetosomes were closely arranged along this magnetosome-associated
62 cytoskeleton, which has been tentatively referred to as "magnetosome filament" (MF)
63 (Frankel and Bazylinski, 2006). It was speculated that magnetosome filaments might be
64 encoded by the *mamK* gene because of its sequence similarity to other cytoskeletal
65 proteins (Grünberg *et al.*, 2004; Schüler, 2004b), which together with other genes
66 relevant for magnetosome formation is part of the large *mamAB* operon in all analyzed
67 MTB (Grünberg *et al.*, 2001; Jogler *et al.*, 2009a; Jogler and Schüler, 2009; Nakazawa
68 *et al.*, 2009; Murat *et al.*, 2010). MamK proteins form a distinct and coherent branch
69 within the large superfamily of prokaryotic actin-like proteins (Alps), which perform
70 diverse functions in cell shape determination, establishment of polarity, cell division,
71 chromosome segregation, and plasmid partition (Carballido-Lopez, 2006; Derman *et al.*,
72 2009).

73 Because of the difficulties with genetic manipulation of MTB, a *mamK* deletion mutant
74 has so far been available only in AMB (Komeili *et al.*, 2006). AMB Δ *mamK* cells had lost
75 their coherent chain-like structure. Instead, groups of few (two to three) neighboring
76 magnetosomes were separated by large gaps and appeared dispersed throughout the
77 cell (Komeili *et al.*, 2006). Cytoskeletal magnetosome filaments could **no longer** be
78 identified in tomograms of mutant cells, indicating that MamK in fact might be the
79 structural element of the magnetosome-associated cytoskeleton. Similar to MreB and
80 other Alps, MamK fusions to GFP displayed a filament-like organization *in vivo* and
81 appeared as spiral or straight lines in cells of AMB (Dye *et al.*, 2005; Pradel *et al.*, 2006).
82 MamK-GFP of AMB expressed in *E. coli* formed straight filaments, which were
83 structurally and functionally distinct from the known MreB and ParM filaments

84 (Carballido-Lopez and Errington, 2003; Pradel *et al.*, 2006). Recombinant MamK of *M.*
85 *magnetotacticum* MS-1 (in the following referred as MS) *in vitro* polymerized into long
86 straight filamentous bundles in the presence of a non-hydrolyzable ATP analogue
87 (Taoka *et al.*, 2007). In the related magnetic bacterium MSR MamK was shown to
88 interact with the acidic repetitive MamJ protein, which was demonstrated to be another
89 key player of magnetosome chain assembly (Scheffel *et al.*, 2006; Scheffel and Schüler,
90 2007). A deletion mutant of *mamJ* did no longer produce straight magnetosome chains,
91 but magnetite crystals were found arranged in compact clusters (Scheffel *et al.*, 2006;
92 Scheffel and Schüler, 2007), whereas empty vesicles and immature crystals are
93 scattered throughout the cytoplasm and detached from the magnetosome filaments,
94 which were still present within MSR Δ *mamJ* cells.

95 One obvious model that was suggested from these data is that MamJ connects
96 magnetosomes to the cytoskeletal MF formed by MamK, which mechanically stabilizes
97 the magnetosome chain and prevents it from collapsing (Komeili, 2006; Komeili, 2007;
98 Scheffel and Schüler, 2007). According to this model, loss of either MamK or MamJ
99 should result in an essentially identical phenotype, which is the abolishment of chain
100 formation and agglomeration of magnetosome particles. However, the reported
101 phenotypes of the MamJ deletion in MSR (agglomerated magnetosomes) and the
102 MamK deletion in AMB (dispersed magnetosomes) were [strikingly](#) distinct. [This raised](#)
103 [the question, whether the MamJ and MamK proteins perform different or additional](#)
104 [functions in different species of MTB, and whether the observed phenotypic differences](#)
105 [are due to species-specific modes of chain formation caused by different genetic control](#)
106 [in the two strains used in the two studies \(Jogler and Schüler, 2007; Komeili, 2007\). In a](#)
107 [very recent study, a second actin-like protein was discovered in the genome of AMB that](#)

108 shares 54.4% identity with MamK and is encoded within a genomic islet outside the MAI
109 (Rioux *et al.*, 2010). Like MamK, this MamK-like protein was also demonstrated to form
110 filaments both *in vivo* and *in vitro*, and it was speculated that the presence of this second
111 *mamK*-like gene might account for the variable phenotype of the Δ *mamK* mutant in AMB
112 (Rioux *et al.*, 2010).

113 To reconcile these conflicting observations and to further clarify the role of MamK, we
114 characterized in detail a *mamK* deletion mutant of MSR by TEM and CET. We show that
115 in contrast to AMB, MamK of MSR is not required for chain formation. However, the
116 absence of magnetosome filaments results in a pleiotropic phenotype displaying shorter
117 and fragmented chains that are displaced from their usual midcell localization. In
118 addition, mutants are also impaired in magnetite formation. Our results suggest that
119 MamK has a role in magnetosome chain positioning and MM vesicle formation, and loss
120 of MamK may have distinct effects in different bacteria depending on the genetic
121 context.

122

123 Results

124 Characterization of an unmarked, in-frame $\Delta mamK$ mutant of *M. gryphiswaldense*

125 We generated an unmarked, in-frame *mamK* deletion mutant of *M. gryphiswaldense*
126 (MSR), in the following referred to as MSR $\Delta mamK$. Under standard conditions
127 (microaerobic, 30 °C) cells of MSR $\Delta mamK$ strain exhibited morphology (Fig. 1), as well
128 as growth and motility apparently identical to the wildtype (WT). Whereas single
129 crossover insertants of pEK32 were deficient in magnetite crystal formation,
130 MSR $\Delta mamK$ cells formed magnetosomes and aligned to magnetic fields. However,
131 magnetic orientation of mutant cultures was markedly weaker than the WT as indicated
132 by lower C_{mag} values (1.08 vs. 1.44 in the WT). Measurement of ~ 590 magnetosomes
133 from ~ 30 cells revealed that the magnetite crystals were unaffected in shape and size,
134 and the mean crystal diameter of 34 nm was essentially identical to that of the WT
135 (33 nm). However, on average MSR $\Delta mamK$ cells contained substantially fewer
136 magnetosomes (19.7 crystals) per cell than WT cells (35.3 crystals) (Fig. 1D*iv*) grown
137 under identical conditions, which was also consistent with a reduced iron accumulation
138 of mutant cells (30.4 $\mu\text{g}/\text{mg}$ vs. 51.7 $\mu\text{g}/\text{mg}$ dry weight in the WT, Fig. 1D*v*).

139 Chain formation was assessed by TEM with respect to the average number of chains
140 per cells, the average length (i. e. the number of particles), and the average distance
141 between neighboring particles. A chain was defined empirically by a minimum number of
142 10 magnetosomes that showed a linear alignment, and which were interspaced by not
143 more than ~ 50 nm from each other. Within this distance magnetic crystals are known to
144 interact magnetically, whereas single particles spaced by about >200 nm are
145 magnetically uncoupled and behave as independent magnetic dipoles (Simpson, 2008;
146 Li *et al.*, 2009). Around 70% of WT magnetosome chains had between 19 and 44

147 particles, were 0.6 to 2.5 μm in length, tightly spaced (10.9 nm interparticle distance,
148 50.2 nm center-to-center distance), with smaller, apparently growing, and more widely
149 spaced magnetite particles at the ends. In 92% of the cells straight, long, and
150 continuous chains were positioned at midcell (Fig. 1Ciii). Ectopic (e. g. terminal) chain
151 localization or fragmented chains (6%) were found only occasionally. However, in about
152 17% of the WT cells 2-3 parallel chains were observed (Fig. 1Ai-ii).

153 In contrast, $\text{MSR}\Delta\text{mamK}$ cells displayed a distinct and much more inconsistent pattern
154 of magnetosome chain configurations. A fraction of cells had lost their coherent, tightly
155 spaced chain-like structure, but instead magnetosomes were dispersed along a linear
156 axis throughout the cells and spaced by distances up to ~ 920 nm (Fig. 1B, C).

157 However, this pattern, which was somewhat reminiscent to the described phenotype of
158 ΔmamK in AMB (Komeili *et al.*, 2006) was found in only 18% of the cells (Fig. 1Bii).

159 Instead, the major fraction of cells still formed single or multiple tightly spaced chains. A
160 minor fraction (5%) of the $\text{MSR}\Delta\text{mamK}$ cells exhibited chains similar to those in the WT
161 (i. e., one single, tightly spaced chain with >10 magnetosome positioned at midcell; Fig.
162 1Ciii). In the majority of cells, however, chains were aberrant with respect to their
163 number, length, and position. For example, the occurrence of fragmented chains with
164 multiple (up to 4) subchains was increased (average 1.38 chains per $\text{MSR}\Delta\text{mamK}$ cell)
165 compared to the WT (1.19 per cell). Individual fragmented chains on average were
166 significantly shorter (14.2 particles in $\text{MSR}\Delta\text{mamK}$ vs. 26.1 in the WT), and 29% of the
167 cells had chains with fewer than 10 particles, compared to only 2% in the WT. Notably,
168 parallel chains that were frequently present in WT cells, were never observed in
169 $\text{MSR}\Delta\text{mamK}$ cells. The position of magnetosome chains within cells was estimated by
170 dividing the cells into three equal sectors to distinguish between midcell and terminal

171 localization. A midcell localization of the chain was observed in only 43% of
172 MSR Δ *mamK* cells (WT: 92%), whereas in the majority of mutant cells the chains were
173 located closely to the cell poles (Fig. 1C*i-ii*).

174 We and others had observed previously that purified magnetosome particles from WT
175 cells tend to form chains *in vitro* as long as the particles are enveloped by an intact
176 magnetosome membrane (MM) (Grünberg *et al.*, 2004; Kobayashi *et al.*, 2006; Scheffel
177 *et al.*, 2006; Taoka *et al.*, 2007; Li *et al.*, 2009). To test whether the loss of MamK, which
178 is associated with the MM of MSR (Fig. S1), had an effect on the integrity of the MM,
179 and consequently, on chain formation *in vitro*, magnetosome particles purified from
180 mutant and WT cells were investigated by TEM. Isolated mutant and WT magnetite
181 crystals were surrounded by a MM-like organic layer of identical thickness (8-12 nm) and
182 appearance as reported previously (Gorby *et al.*, 1988; Schüller, 2004a; Taoka *et al.*,
183 2006) with junctions that interconnected the individual particles (Fig. S2). Similar like WT
184 magnetosomes, isolated mutant magnetosomes had a tendency to form chains as
185 observed before (Grünberg *et al.*, 2004) (Fig. S2*iii-iv*).

186

187 **Complementation analysis: MamK_{MSR} and MamK_{AMB} are functionally equivalent**

188 Immunodetection revealed that MamM and MamB, whose genes are located 338 and
189 7192 bp downstream of *mamK* within the *mamAB* operon, respectively, were expressed
190 at WT levels in the mutant strains (data not shown), indicating that *mamK* deletion had
191 no polar effects. To further preclude second-site mutations, we analyzed cells
192 transcomplemented with a functional *mamK* gene. Cloning and expression of the 1044
193 bp *mamK*_{MSR} gene under control of the native P_{*mamAB*} promoter (Lang *et al.*, 2009) in
194 pEK36 resulted in MamK expression comparable to WT levels (data not shown) upon

195 transfer into $MSR\Delta mamK$. In addition, also magnetite formation, iron accumulation and
196 chain formation were restored, albeit to a lower extent than in the WT (Fig. 1D*iv-v*, 4*iv*).
197 To answer the question whether observed differences in WT and $\Delta mamK$ phenotypes
198 between AMB and MSR might be due to sequence divergence of MamK orthologs, we
199 also tested transcomplementation by $mamK_{AMB}$, and in addition by $mamK_{MS}$ (*M.*
200 *magnetotacticum* MS-1). Plasmids pEK37 and pEK35 carrying $mamK_{AMB}$ and $mamK_{MS}$,
201 respectively, were conjugated into $MSR\Delta mamK$. Magnetosome numbers, iron
202 accumulation, C_{mag} and chain formation were restored by $MSR\Delta mamK+pEK35$ (data not
203 shown) and $MSR\Delta mamK+pEK37$ (Fig. 1D*iii-v*) at comparable levels, indicating that
204 $mamK_{MS}$ and $mamK_{AMB}$ are functionally equivalent to $mamK_{MSR}$ and can substitute its
205 function in $MSR\Delta mamK$ cells. We also investigated the effect of MamK overexpression
206 by cloning of $mamK_{MSR}$ on pEK33 under control of the strong MSR promoter $pmamDC$
207 (Lang *et al.*, 2009). Transmission electron micrographs revealed long, straight WT-like
208 magnetosome chains in MSR cells expressing $mamK$ from pEK33, and filaments of
209 similar abundance, length, and thickness were visible within 3D maps. Likewise, cells
210 displayed similar magnetosome numbers (Fig. 1D*i-v*) and magnetic orientation (WT
211 $C_{mag}=1.47$, WT + pEK33 $C_{mag}=1.50$), indicating that moderate overexpression of $mamK$
212 has only minor effects on magnetosome chain formation (Fig. S3).

213

214 Intracellular localization of MamK

215 Plasmids harboring various MamK-EGFP fusions were expressed in WT and several
216 mutant backgrounds. Functionality of fusions was verified by partial restoration of WT-
217 like phenotype upon expression of pAS_K, pAS_K1, pAS_K2 and pEK42 in
218 $MSR\Delta mamK$. Fluorescence microscopy revealed distinct localization patterns from

219 linear to helical filaments in all tested MamK-EGFP fusions. However, the respective
220 patterns were dependent on the length of the linker between EGFP and MamK:
221 Expression of pAS_K1 harboring a C-terminal MamK-GSI-EGFP (Fig. 2*i-ii*) fusion, and
222 pAS_K2 harboring an N-terminal EGFP-SAI-MamK fusion (data not shown) resulted in a
223 linear fluorescence signal of about half the cell length that was restricted to midcell in *E.*
224 *coli* and MSR, similar as observed in other studies (Pradel *et al.*, 2006). In contrast,
225 WT+pAS_K harboring a N-terminal EGFP-LCLQGE-MamK displayed a linear-to-helical
226 fluorescence pattern spanning from pole to pole throughout the entire cell, and
227 occasionally forming loops (Fig. 2*iii*). A similar pattern was also observed if pAS_K and
228 pEK42 were expressed in MSR Δ *mamK*, the non-magnetic mutant strain MSR-1B
229 lacking most magnetosome genes by deletion (Schübbe *et al.*, 2003; Ullrich *et al.*,
230 2005), and *E. coli* (Fig. 2*iv-viii*). Previous experiments indicated that MamK interacts with
231 the acidic MamJ protein (Scheffel *et al.*, 2006; Scheffel and Schüler, 2007), but the
232 filamentous localization of MamK was independent from MamJ (as demonstrated by
233 expression in Δ *mamJ* strain) and other magnetosome genes (as demonstrated by
234 expression in MSR-1B) (Scheffel *et al.*, 2006). Therefore, we asked whether localization
235 of MamJ was on the other hand dependent on the presence of MamK. Expression of
236 pAS_J harboring a MamJ-EGFP fusion in MSR Δ *mamK* abolished its filamentous
237 localization, but instead resulted in a punctual, cytoplasmic fluorescence signal, similar
238 as the localization of MamJ-EGFP previously detected in MSR-1B (Scheffel *et al.*,
239 2006)(Fig. 2*ix-x*). This indicates that proper MamJ localization requires the presence of
240 MamK. Since the linear to helical localization of EGFP-MamK (pAS_K, pEK42) was also
241 observed in *E. coli* and *M. gryphiswaldense* MSR-1B backgrounds (Fig. 2*vii-viii*), [this](#)
242 [demonstrates](#) that the filamentous localization is an intrinsic property of EGFP-

243 MamK_{MSR}, which does not require the presence of other magnetosome proteins.
244 Expression of pAS_K in AMB resulted in the same filamentous signal pattern, however,
245 spiral localization was absent (Fig. 2xi).
246 Spontaneous formations of spheroplasts (“cocoid bodies”) can be regularly observed in
247 aging cells of *M. gryphiswaldense* and other magnetospirilla (Balkwill *et al.*, 1980;
248 Schüler and Köhler, 1992). Interestingly, in such spheroplast cells EGFP-MamK
249 (pAS_K) did no longer localize within linear filaments, but instead yielded a ring-like
250 fluorescence signal closely beneath the cell periphery, which is consistent with the
251 peripheral ring-like, bent appearance of the magnetosome chains in such a cell as
252 shown by fluorescence microscopy and TEM (Fig. 2xii-xiii).

253

254 **Cryo-electron tomography (CET)**

255 Previous CET analyses of magnetosome chain topology in AMB and MSR were limited
256 to only single or a few cells (Komeili *et al.*, 2006; Scheffel *et al.*, 2006). Therefore, we
257 analyzed chain assembly and magnetosome filaments in greater detail in a larger
258 number of WT and MSR Δ *mamK* cells of MSR. Filaments accompanying the
259 magnetosome chains were identified in 16 of 28 of all analyzed tomographic volumes
260 from WT cells (Fig. 3ii-viii), and 2 of 10 analyzed MSR Δ *mamK* cells complemented with
261 pEK42 (*mamK*_{MSR}, Fig. 4iv) and pEK34 (*mamK*_{AMB}). Since tomograms at the recorded
262 magnification are limited in the field of view, they represent only a fraction of the whole
263 cell. Moreover, some information is not accessible due to the limited tilt range and the
264 resulting missing wedge. Therefore it is possible that filaments in the other WT and
265 transcomplemented cells escaped detection if localized perpendicular to the tilt-axis.
266 Individual filaments, which were 3 - 6 nm in diameter and 0.5 - 1 μ m in length,

267 occasionally formed bundles of 2 - 4 filaments that were ~ 20 nm in diameter and
268 approximately 1 μ m long (Movie S1). However, since filaments were not always within
269 the same z-plane, their total dimensions can only be roughly estimated. Detected
270 filaments were localized within the cytoplasm in close proximity to MM vesicles.
271 Although the magnetosome chains were predominantly found at midcell, empty vesicles
272 and filaments were also present in 100 – 300 nm vicinity to the inner membrane of the
273 cell pole. However, we were unable to detect direct connections or discern distinct
274 structures where filaments insert into the polar membrane. This was partially due to the
275 presence of complex ordered structures resembling arrays of chemoreceptors (Briegel
276 *et al.*, 2009), which were located closely beneath the polar membrane (Fig. 3vii-viii).
277 Analysis of different CET datasets determined an array length of ~ 28 nm and a lattice
278 distance of ~ 11 nm (Fig. 3viii, insets). Notably, in some cells filaments seemed to be
279 connected laterally to the CM.
280 A couple of WT and transcomplemented cells were tomographed in state of early (Fig.
281 3iv-v), and late division (Fig. 4iv). According to those tomograms, the MF traverse the
282 entire cell before septum formation, which remarkably might occur asymmetrically from
283 only one side (Fig. 4iv). During later division the magnetosome chain, and likely also the
284 magnetosome filament may be split into two parts (Fig. 3iv-v, 4iv). However, due to the
285 potential risk of technical artifacts these observations require future verification.
286 Interestingly, two distinct filaments were detected in fig. 4iv within this cell. This was not
287 observed in the analyzed WT cells and might be the result of *mamK* expression from
288 pEK42.
289 As in conventional micrographs, tomograms of WT cells frequently showed two parallel
290 chains of particles that were aligned opposite to each other along the filaments (Fig. 1Ai,

291 [3i-v](#)). In contrast, we failed to detect parallel chains in any of the 15 analyzed
292 MSRΔ*mamK* tomograms, which always contained only one linear string of crystals per
293 analyzed section.

294 Sometimes filaments with association to the CM were detected, where magnetosomes
295 were absent or sparse (Fig. [3iii](#)). Whereas the number of magnetite crystals was
296 significantly lower in MSRΔ*mamK*, the proportion of empty vs. filled vesicles per
297 tomographed area was not increased. Even though the absolute enumeration of
298 vesicles per cell is not possible due the limited analyzed area and technical limitations
299 (e.g. limited tilt range, missing wedge), the total number of MM vesicles (empty or filled)
300 per viewed section was also decreased in the mutant. If all tomograms of central
301 sections at identical magnification were taken into account under the assumption that
302 they may represent comparable, randomly chosen areas at midcell from the WT (15
303 cells) and MSRΔ*mamK* (8 cells) cells, the average number of all vesicles were 21.6
304 (WT) vs. 14.8 in the mutant, respectively, implying that the formation of MM vesicles is
305 affected in the mutant.

306 MM vesicles were predominantly found in close contact with the CM. In several cells,
307 empty MM vesicles were detected that were invaginating from the CM, apparently with
308 the MM forming a continuum with the CM (Fig. [3iv](#), inset). The size of empty or partially
309 filled vesicles varied between 13.4 and 33.5 nm. However, vesicle dimensions were not
310 strictly correlated with the presence or absence of growing immature crystallites, as
311 larger vesicles (18 - 33.5 nm) devoid of crystals as well as smaller vesicles harboring
312 small crystallites were apparent in the analyzed tomograms.

313

314 **Effect of MSRΔ*mamK* on dynamic assembly of magnetosome chains**

315 Deletion of *mamK* did not result in agglomeration of magnetosomes, but mutant cells still
316 maintained a chain-like configuration. We therefore reasoned that instead merely
317 providing a backbone or scaffold that mechanically stabilizes the magnetosome chain,
318 the primary function of MamK might be rather in the control of the dynamic positioning
319 and concatenating the individual particles during chain assembly and cell division as
320 speculated before (Frankel and Bazylinski, 2006; Pradel *et al.*, 2006). For clarification,
321 we undertook a growth experiment in which magnetite synthesis was induced in growing
322 MSRΔ*mamK* and WT cells by the addition of iron to previously non-magnetic, iron-
323 starved cells. As shown in Fig. 5, both WT and MSRΔ*mamK* cells started to form
324 magnetite after addition of 50μM Fe(III)-citrate, and small (10 – 20 nm) crystallites could
325 be first detected after 30 min. As in previous induction experiments (Scheffel *et al.*,
326 2006; Faivre *et al.*, 2007), initiation of magnetosome formation took place usually at few
327 locations close to the cell periphery and scattered throughout the cell in WT and
328 MSRΔ*mamK*. During the first 80 min magnetite biomineralization proceeded at similar
329 rates in both strains. After about 100 min, magnetite formation of the mutant then lagged
330 behind the WT, resulting in a lower magnetic orientation for the MSRΔ*mamK* over the
331 remaining 200 min (Fig. 5). After 90 min irregular chains of magnetosomes became
332 apparent at different loci in both mutant and WT cells. However, while WT cells formed
333 the typical linear, and sometimes parallel chain fragments already located at midcell,
334 chains in induced MSRΔ*mamK* mutant cells were displaced, short and more distorted
335 than in those WT cells. After 120 and 300 minutes, further development of WT chains
336 resulted in gradual extension and midcell localization, whereas in MSRΔ*mamK* cells
337 fragmented, displaced chains were formed.

338 Discussion

339 Previous studies had suggested that the actin-like protein MamK is required for
340 magnetosome chain assembly of AMB by aligning these organelles within the cell
341 (Komeili *et al.*, 2006; Pradel *et al.*, 2006). However, the phenotype of a $\Delta mamK$ mutant
342 of MSR generated in this study argues against an essential role in chain formation in this
343 organism, since in spite of the absence of filamentous structures mutant cells are still
344 able to form linear and coherent chains, albeit with reduced lengths and ectopic
345 positions. For the assembly of an functional magnetosome chain, individual magnetite
346 crystals have to be (i) aligned along a common linear axis, (ii) concatenated (i. e. by
347 bringing newly synthesized particles to the nascent, tightly spaced magnetosome chain),
348 and finally, (iii) chains have to positioned properly at their usual midcell localization.
349 Instead merely providing a backbone or scaffold that mechanically stabilizes
350 magnetosome chain, our data support speculations that MamK might be involved in
351 sorting, concatenating and intracellular positioning of the magnetosome chain (Pradel *et*
352 *al.*, 2006; Jogler and Schüler, 2009). On the other hand, the fact that a small percentage
353 of $\Delta mamK$ cells still form long chains does not necessarily indicate that MamK has no
354 scaffolding role at all, but just could mean that it cannot be the only factor promoting
355 chains.

356 Our induction experiments show that MSR $\Delta mamK$ cells are also still able to assemble
357 short, but coherent chains from dispersed magnetosome particles if challenged with the
358 *de novo* synthesis of magnetite particles in non-magnetic, iron-starved cells undergoing
359 cell division. This raises the question of how these chains are maintained in
360 MSR $\Delta mamK$ mutants against their immanent tendency to agglomerate. Several
361 mechanisms for chain formation have been suggested. In AMB chain initiation starts

362 with the simultaneous formation of multiple, adjacent magnetosomes (Komeili *et al.*,
363 2004; Li *et al.*, 2009). In marked difference, magnetite biomineralization in MSR is
364 initiated at multiple sites dispersed over the entire cell (Scheffel *et al.*, 2006) before
365 eventually becoming concatenated into the mature coherent chains located at midcell,
366 which suggests a control over dynamic localization and intracellular positioning of
367 magnetosomes in this organism. When magnetic crystals continue to grow, increasing
368 magnetostatic interactions between adjacent particles force them into close contact,
369 which is then further stabilized by interactions through MM constituents. In the absence
370 of the “bead-on-a-string” like alignment along the MamK filaments, connections between
371 the invaginating MM vesicles and the CM may be sufficient to maintain the linear
372 arrangement of subchains in MSR Δ *mamK*. In addition to the cytoskeletal magnetosome
373 filament, an elusive sheath-like structure has been postulated that may hold
374 magnetosome chains together and in place within the cell (Kobayashi *et al.*, 2006;
375 Taoka *et al.*, 2006). However, in our extensive CET studies we failed to detect any
376 indications for the existence of such an intracellular structure.

377 Like in AMB, deletion of the *mamK* gene resulted in the complete absence of
378 magnetosome filaments. In addition, we were unable to detect any other filament-like
379 structures in MSR Δ *mamK* cells. This is interesting, as MSR Δ *mamK* cells are likely to
380 contain further cytoskeletal structures formed by other filamentous proteins, such as
381 MreB and FtsZ, which are encoded in the genome of MSR. In a study on *C. crescentus*,
382 in which the formation of MreB filaments was inhibited by A22 treatment, similar
383 filaments, which were speculated to be FtsZ, were still detectable by CET (Li *et al.*,
384 2007). Our failure to detect them thus might indicate that other cytoskeletal structures
385 are way less abundant than MamK filaments within the cell.

386 Complementation of the $MSR\Delta mamK$ mutant not only with $mamK_{MSR}$, but also with
387 $mamK_{AMB}$ and $mamK_{MS}$ did restore chain formation and the presence of magnetosomal
388 filaments, indicating that these *mamK* alleles have equivalent functions and can substitute
389 each other. However, despite the morphological and ultrastructural resemblance of the
390 two organisms, the phenotypes of *mamK* mutants are distinct between MSR and AMB.
391 Whereas the effect on chain assembly is less pronounced in $MSR\Delta mamK$ than in
392 $AMB1\Delta mamK$, in which the mutant lacked the long, highly organized chains seen in WT
393 (Komeili *et al.*, 2006), loss of MamK in MSR has several additional, pleiotropic effects.
394 These differences do not result from different growth conditions, as MSR grown in
395 MSGM (i. e. the genuine AMB medium) displayed the same morphology and
396 magnetosome organization as in FSM medium (data not shown). On the other hand, WT
397 AMB cells grown in FSM medium under identical conditions as MSR display a distinct
398 chain configuration that is characterized by fairly loose, widely spaced chains that may
399 extend through the entire cell (Fig. S4), compared to the midcell localization of densely
400 spaced MSR chains (Fig. 1A), and it has been recently argued by Rioux *et al.* that the
401 fraction of misaligned magnetosome chains in $AMB1\Delta mamK$ may be well within the
402 variability usually observed in the WT strain (Rioux *et al.*, 2010). This relatively weak
403 phenotype and the differences between MSR and AMB might be explained by the fact
404 that only 52% of all genes are shared between the two strains (Richter *et al.*, 2007). In
405 fact, in the recent study by Rioux *et al.* a second *mamK*-like gene was discovered
406 outside the MAI in an islet together with 6 additional magnetotaxis related genes (Rioux
407 *et al.*, 2010). These findings support the idea that the observed differences between
408 AMB and MSR and their *mamK* mutants are due to a different genomic context.

409 Therefore, only a double deletion mutant of the *mamK*-like gene in addition to Δ *mamK*
410 will reveal a more conclusive picture about MamK function in AMB.

411 One of the various effects of the *mamK* deletion in MSR is the formation of multiple,
412 fragmented chains, which are strongly reminiscent to the subchains observed by Li *et al.*
413 in experiments, in which magnetite formation was induced in aerobically grown non-
414 magnetic cells of AMB by a shift to microaerobic incubation (Li *et al.*, 2009). Each of
415 these subchains behaved as an ideal uniaxial single-domain particle with extremely
416 weak magnetostatic interactions between subchains (Li *et al.*, 2009). Another distinctive
417 feature of the MSR mutant is that the chains are displaced from their usual midcell
418 location, which indicates that MamK is involved in positioning of magnetosomes by an
419 as yet unknown mechanism. It has been speculated that positional information might be
420 provided possibly by interaction with the divisome machinery that regulates proper cell
421 division and determines septum formation (Schüler, 2008; Adams and Errington, 2009).
422 This hypothesis has been further stimulated by the fact that a second *ftsZ*-like gene has
423 been identified in the *mamXY* operon of MSR (Richter *et al.*, 2007). A putative chimeric
424 protein was found within a metagenomic clone, in which a MamK-like domain is coupled
425 to an FtsZ-like domain (Jogler *et al.*, 2009b). A recent study has shown that the second
426 FtsZ-like protein in MSR is not involved in cell division but had rather an effect on
427 biomineralization and, apparently, also on chain assembly (Ding *et al.*, 2009). So far, it
428 still remains to be analyzed whether this or the genuine FtsZ has an effect in providing
429 information about midcell position.

430 Previous studies of MamK_{AMB} localization by Komeili *et al.* revealed that a C-terminal
431 GFP fusion appeared in straight lines extending across most of the cell approximately
432 along its inner curvature, consistent with the magnetosome-associated filaments in both

433 localization and extent (Komeili *et al.*, 2006). CET revealed networks of long filaments
434 200 to 250 nm in length running parallel along the chain of an AMB WT cell. At any
435 position within the chain, up to seven of these filaments flanked the magnetosome with
436 no obvious spatial pattern (Komeili *et al.*, 2006). In contrast, fluorescence microscopy in
437 our study revealed a more variable localization pattern of MamK_{MSR} depending on the
438 particular GFP fusion and linker length. Variable fluorescence patterns were also
439 detected for other actin-like proteins like ParM and MreB (Jones *et al.*, 2001; Møller-
440 Jensen *et al.*, 2002), as incorporation of EGFP into a polymeric structure might affect
441 MamK tertiary structure. Thus, a longer linker might provide sterical freedom required for
442 its native localization. **In addition, different linkers might affect the stability of EGFP**
443 **fusions, and therefore, the distinct localization of the MamK fusions might also be**
444 **function-unrelated.** Although MamK-EGFP fusions (pAS_K1/2), which show midcell
445 fluorescence, also seem to complement the deletion of *mamK*, the pole-to-pole
446 localization observed for EGFP-MamK (pAS_K, pEK42) is more consistent with the
447 polar localization of MF bundles observed by CET, and also with the observation by
448 Pradel *et al.* that one extremity of MamK_{AMB} was located at the pole if expressed in *E.*
449 *coli* (Pradel *et al.*, 2006; Pradel *et al.*, 2007). It has been also suggested by these
450 authors that MamK might somehow be involved in magnetoreception, possibly by
451 interaction with other polar components (*lcsA*) (Pradel *et al.*, 2006). Our finding that
452 extremities of MamK in some MSR cells extend towards arrays of **chemoreceptors**
453 would support a possible interaction between *mamK* and these structures in signal
454 transduction.

455 It has been demonstrated previously that MamK interacts with MamJ, but MamJ is not
456 required for MamK filament formation (Scheffel *et al.*, 2006; Scheffel and Schüler, 2007).

457 We found that on the other hand MamK is required for the filamentous localization of
458 MamJ-EGFP (Fig. 2ix-x), which is abolished in the $MSR\Delta mamK$ mutant. Previous
459 studies have suggested that MamJ attaches magnetosomes to filaments formed by
460 MamK by direct interaction (Scheffel and Schüler, 2007). If this would be the only MamJ
461 function, then loss of either MamJ or MamK would be expected to result in essentially
462 identical phenotypes, which is the collapse of chains and agglomeration of
463 magnetosomes. As chain configuration, however, is maintained even in the absence of
464 MamK, but not MamJ, the mode of chain stabilization by MamJ cannot exclusively be
465 accomplished by MamK interaction, but has to involve other, so far unknown
466 mechanisms as well.

467 $MSR\Delta mamK$ chains are also shorter, presumably as a consequence of the decreased
468 numbers of magnetite crystals in the mutants. At this point, the reason for this
469 unexpected effect on magnetosome formation is not clear. It has been suggested that
470 MamK could act through establishment of magnetosome biogenesis factors (Komeili,
471 2007). This might be, for example, by mediating the recruitment of other proteins
472 required for biomineralization to the MM. A role in the recruitment and positioning of
473 particular proteins has been demonstrated for other Alps and tubulin-like proteins, such
474 as FtsZ, ParM and MreB, in *B. subtilis* and *E. coli* (Salje and Löwe, 2008; Adams and
475 Errington, 2009; Gamba *et al.*, 2009; Vats *et al.*, 2009). However, a preliminary
476 comparative analysis of the MM between the mutant and the WT revealed virtually the
477 same band patterns in SDS-PAGE experiments (data not shown). Intriguingly, our data
478 imply that the number of magnetosome membrane vesicles is higher (21.6) in
479 tomograms of the WT compared to 14.8 in the mutant, and the reduced number of MM

480 vesicles in the mutant might be the reason why less magnetosome crystals are formed
481 in cells devoid of MamK.

482 Our extensive CET analysis of > 40 WT and mutant cells also revealed several
483 previously unrecognized ultrastructural features with relevance for magnetosomal
484 organelle formation. For example, we have shown that, like in AMB the MM in MSR
485 invaginates from the CM and at least transiently forms a continuum between the two
486 membranes (Komeili *et al.*, 2006), indicating that the mechanisms of intracellular
487 differentiations are similar between these organisms. In addition, we found that in the
488 WT formation of two parallel chains is rather common, which was never observed in
489 MSR Δ *mamK* cells. The reason for the formation of multiple chains in the WT is not
490 entirely clear, but it can be speculated that MamK filaments may have a strong affinity
491 for binding MM vesicles, possibly by its interaction with MamJ and other proteins, and
492 thus tend to gather magnetosomes within their vicinity.

493 In conclusion, our data argue for a function of MamK in positioning and **concatenating**
494 magnetosome chains rather than merely providing a rigid scaffold for chain alignment.
495 **Our results further suggest that the role of MamK is likely to be more complex and**
496 **somewhat distinct from previously reported models that were mostly inferred from the**
497 **single *mamK* deletion in AMB** (Komeili *et al.*, 2006; Rioux *et al.*, 2010). At this point, the
498 precise mechanisms by which magnetosome chains are positioned by MamK remains
499 elusive and will require further investigation of interaction with and localization of further
500 constituents of the magnetosome assembly and **vesicle formation** machinery.

501

502 **Acknowledgement**

503 We are grateful to Günter Pfeifer (MPI of Biochemistry) for help with the TEM. This work
504 was supported by the Max Planck Society and the Deutsche Forschungsgemeinschaft
505 (Schu1080/9-1 and 10-1).

For Peer Review

506 Experimental procedures

507 **Bacterial strains, media and magnetosome isolation**

508 Strains *M. magnetotacticum* AMB-1 (AMB) and *M. gryphiswaldense* MSR-1 (MSR) were
509 grown in modified liquid FSM medium and LIM (Low iron media, modified FSM) (Faivre
510 *et al.*, 2007). Modified magnetic spirillum growth medium (MSGM) (Blakemore *et al.*,
511 1979; Komeili *et al.*, 2004)(50 μ M ferric citrate instead of ferric malate) was alternatively
512 used where indicated. Growth of *Escherichia coli* strain BW29427 (Tab. 1) was
513 accomplished in lysogeny broth (LB) supplemented with 1 mM DL- α,ϵ -diaminopimelic
514 acid (Sigma-Aldrich, Switzerland). Culture conditions for *E.coli* strains were as described
515 (Sambrook and Russel, 2001). Magnetosomes were isolated from microaerobically
516 grown 5l cultures as described elsewhere (Grünberg *et al.*, 2004; Ohuchi and Schüller,
517 2009). Optical densities and C_{mag} values of MSR cultures were measured
518 turbidimetrically at 565 nm with immotile cells inactivated by the addition of
519 formaldehyde (Fluka, Switzerland) to a final concentration of 0.1% prior to the
520 measurement (Scheffel *et al.*, 2006).

521

522 **DNA techniques and Southern Blot**

523 Total DNA from all strains used in this study was isolated as described previously
524 (Marmur, 1961; Grünberg *et al.*, 2001). Genetic constructs used to generate the
525 MSR Δ *mamK* deletion were amplified using standard PCR procedures. The primers and
526 plasmids used in this study are shown in Table 1. Primer sequences for amplification of
527 DNA fragments from MSR were deduced from GenBank sequence deposition
528 BX571797. The primer pairs used for the amplification of *mamK* from *Magnetospirillum*
529 strains AMB and MS were deduced from sequence deposition NC_007626 and

530 NZ_AAAP01003824.1, respectively. For sequencing, BigDye terminators v3.1 (Applied
531 Biosystems, Darmstadt, Germany) were used. Sequence data were analyzed with
532 Lasergene 6 (DNASTar, Inc., Madison, WI) and MacVector 7.2.3 (Oxford Molecular, Ltd.,
533 Oxford, United Kingdom) programs. Southern blots were performed by standard
534 procedures as described previously (Ullrich *et al.*, 2005) (Fig. S5).

535

536 **Construction of an unmarked in-frame *mamK* deletion mutant**

537 Gene deletion was accomplished via homologous recombination of up- and downstream
538 *mamK* flanking sequence in pEK32 with the MSR chromosome. A 2003 bp upstream
539 and a 2009 bp downstream *mamK* flanking region were amplified with primer pairs
540 EK2_K_u_f /EK_K_u_r and EK_K_d_f/EK2_K_d_r. The fragments were fused by
541 cloning into the *Xba*I and *Bam*HI restriction sites of pK19*mob*GII vector, resulting in
542 pEK32. Plasmids were transferred into *M. gryphiswaldense* by biparental conjugation
543 and screening was performed as previously described (Schultheiss *et al.*, 2004).

544 Screening for the *gusA* marker (Katzen *et al.*, 1999) revealed 8 Kan^R insertion mutants
545 occurring with a frequency of 1.7×10^{-7} on X-Gluc (5-Bromo-4-Chloro-3-Indolyl- β -D-
546 glucuronic acid, 0.5 mM) containing solid FSM plates. After 2 passages for 3 days in 300
547 μ l liquid culture and subsequent 1 day in 10 ml (\sim 5 generations), an incubation for 10
548 days on solid FSM at 30 °C under microoxic conditions was performed. Screening by
549 PCR of 24 white colonies for putative double crossover resolvants revealed 8 positive
550 candidates that were *gusA*⁻ and Kan^S. Double crossover mutants were obtained at a
551 final frequency of 2.6×10^{-3} . Successful unmarked in-frame deletion of *mamK* was
552 confirmed by PCR and Southern blotting using a 816 bp DNA probe amplifying parts of
553 *mamJ* and *mamK* gene of MSR with primer pairs EK_K_f/ EK_probeK02_r (Fig. S5).

554 One clone named MSR Δ *mamK* was selected for further analysis.

555

556 **Complementation experiments**

557 A cloned fragment comprising an open reading frame of 1083 bp that starts with a CTG
558 codon according to the previously deposited database sequence (CAJ30118, (Ullrich *et*
559 *al.*, 2005)) was not functionally expressed (data not shown). Inspection of the aligned
560 sequences of *mamK* nucleotide sequences of *mamK* orthologs from MSR, AMB (1044
561 bp, 33 nt mismatches, 90.8 % aa identity) and MS (1044 bp, 34 nt mismatches, 90.6 %
562 aa identity) revealed a conserved ATG in all three orthologs 39 bp downstream of the
563 predicted CTG start codon in the older database version of *mamK*_{MSR}, which hereafter
564 was considered as the correct start codon, resulting in an open reading frame of 1044
565 bp as in the other strains.

566 The *mamK* gene was either amplified with primer pair EKmamK_F_kurz/EKmamK_R02
567 and the 1056 bp fragment subsequently cloned into *NdeI* and *BamHI* restriction sites of
568 pBBR_{P_{mamDC}} generating pEK36, or with primer pair EKmamK_F02/EKmamK_R02
569 resulting in a 1083 bp fragment in which the start codon CTG was changed into an ATG.
570 Likewise, the ATG defines the recognition site of 5' *NdeI* restriction enzyme. Together
571 with the 3' *BamHI* recognition site the fragment was cloned into pBBR1*pmamAB* (Lang
572 *et al.*, 2009) yielding pEK36 and subsequently transformed into MSR Δ *mamK* via
573 biparental mating as described (Schultheiss and Schüler, 2003; Schultheiss *et al.*,
574 2004). The *mamK* of AMB was PCR amplified with primer pairs
575 EK_mamK_AMB1_F/EK_mamK_AMB1_R2 yielding a 1056 bp fragment which was
576 cloned into *NdeI*/*BamHI* restriction site of pBBR1*pmamAB* or pBBR*pmamDC*, resulting

577 in pEK37 and pEK34, respectively. Amplification and subsequent cloning of MS *mamK*
578 into pBBR1p*mamDC* resulted in pEK35.

579

580 **Construction of Mam-EGFP fusions**

581 Several different *mamK-egfp* (enhanced GFP) expression fusions were constructed via
582 fusion PCR (Ho *et al.*, 1989). The *mamK* gene of MSR (accession number CAJ30118)
583 and *egfp* (pEGFP-N2, Clontech) were amplified using primers as described, resulting in
584 the C-terminal MamK fusion pAS_K1 (Scheffel, 2007). For construction of the N-terminal
585 fusion with a 6 amino acid linker sequence, primer pairs for *egfp*-gene ASEGFP_f10/
586 ASEGFP_r11, and for *mamK* ASmamKs_f3/ ASmamKe_r2, were used and resulted in
587 pAS_K vector (Scheffel, 2007).

588

589 **Gel electrophoresis and Western Blot experiments**

590 Protein concentrations were determined with a BCA-Protein Micro assay kit (Pierce)
591 according to the manufacturer's instructions. For one-dimensional SDS-PAGE of
592 magnetosome-associated proteins we used the procedure of Laemmli (Laemmli, 1970).
593 An amount of magnetosome particles or solubilisate equivalent to 6.5 µg of protein was
594 mixed with electrophoresis sample buffer containing 2% (wt/wt) SDS and 5% (wt/vol) 2-
595 mercaptoethanol. After boiling for 5 min, samples were centrifuged for 3 min. The
596 supernatants were loaded onto polyacrylamide gels containing various concentrations of
597 polyacrylamide (8 to 16%). The non-magnetic fraction of whole cells was further
598 processed as described elsewhere (Grünberg *et al.*, 2001), and 6.5 µg protein were
599 used for analysis on SDS gels. Western Blot experiments were performed as explained
600 in previous work (Schübbe *et al.*, 2006). The anti-MamK primary antibody was raised by

601 S. Schübbe as described (Schübbe, 2005).

602

603 **Fluorescence microscopy**

604 MSR WT and MSR Δ *mamK* bearing the plasmids pAS_J, pAS_K(1,2), were grown in 15
605 ml polypropylene tubes with sealed screw caps and a culture volume of 10 ml to
606 stationary phase. The cell membranes were stained with the membrane stain FM4-64
607 (Invitrogen, Karlsruhe, Germany) at a final concentration of 16.4 μ M, immobilized on
608 agarose pads (FSM salts in H₂O, supplemented with 1% agarose), and imaged with an
609 Olympus BX81 microscope equipped with a 100 UPLSAPO100XO objective (numerical
610 aperture of 1.40) and a Hamamatsu Orca AG camera. Images were captured and
611 analyzed using Olympus cellTM software.

612

613 **Transmission electron microscopy and Cryo-electron tomography**

614 For transmission electron microscopy (TEM) analysis, unstained cells were adsorbed on
615 carbon coated copper grids and air-dried (Plano, Wetzlar). Bright field TEM was
616 performed on a FEI Tecnai F20 transmission electron microscope (FEI; Eindhoven, The
617 Netherlands) at an accelerating voltage of 200 kV. Images were captured with a FEI
618 Eagle 4096 x 4096 pixel CCD camera using EMMenue 4.0 and FEI's Explore 3D.
619 For cryo-electron tomography, a FEI Tecnai F30 Polara transmission electron
620 microscope (FEI; Eindhoven, The Netherlands), equipped with 300 kV field emission
621 gun, a Gatan GIF 2002 Post-Column Energy Filter, and a 2048 x 2048 pixel Gatan CCD
622 Camera (Gatan; Pleasanton, CA) was used. All data collection was performed at 300
623 kV, with the energy filter operated in the zero-loss mode (slit width of 20 eV). Tilt series
624 were acquired using Serial EM (Mastronarde, 2005) and FEI's Explore 3D software.

625 Quantifoil copper grids (Quantifoil Micro Tools GmbH, Jena) were prepared by placing a
626 5 μ l droplet of 10 – 15 nm colloidal gold clusters (Sigma) on each grid for subsequent
627 alignment purposes. A 5 μ l droplet of a fresh MSR culture was added onto the prepared
628 grid, and after blotting was embedded in vitreous ice by plunge freezing into liquid
629 ethane (temperature ca. -170 °C). Single-axis tilt series for tomography were typically
630 recorded with 2° increments over an angular range of +/- 65°. To minimize the electron
631 dose applied to the ice-embedded specimen, data were recorded at low-dose conditions
632 by using automated data acquisition software. The total dose accumulated during the tilt
633 series was kept below 100 e/Å². To account for the increased specimen thickness at
634 high tilt angles, the exposure time was multiplied by a factor of 1/cos α . The object pixel
635 size in unbinned images was 0.661 at a magnification of 34000 x, 0.805 at 27500 x and
636 0.979 at 22500 x. Images were recorded at nominal defocus values of -8 μ m or -4 μ m.

637

638 **Data analysis**

639 Three-dimensional reconstructions from tilt series were performed with the weighted
640 back-projection method and further analysis of the tomograms was done using the TOM
641 toolbox (Nickell *et al.*, 2005). Visualizations of the tomograms were done with Amira
642 (<http://www.amiravis.com>) on 2 times binned volumes.

643

644 **Determination of iron content by atomic absorption spectroscopy (AAS)**

645 Cells were grown to an optical density of 0.2 and aliquots of 1 ml were taken and
646 pelleted. After a subsequent pellet washing step in 0.5 ml 20 mM HEPES + 5mM EDTA
647 both the supernatant (900 μ l) and the pellet were supplemented with 10 μ l and 100 μ l
648 % nitric acid, respectively. Incubation at 98 °C for 2 h dissolved all organic material and

649 magnetosomes, and dilutions of 1:100 and 1:1000 in H₂O were analyzed by AAS
 650 (Varian AA240) using SpectrAA 240FS software version 5.01 (Varian, Australia) with the
 651 following parameters set: wavelength 248.3 nm, slit width 0.2 nm, cathode lamp current
 652 10.0 mA.

653

654 **Table 1: Plasmids, primers and strains used in this work**

655	Vector	Details	Reference	Index
656	pEK32	4kb flanking sequences of <i>mamK</i> [13]	this work	[1]
657	pEK33	<i>mamK</i> _{MSR-1} [15]	this work	[2]
658	pEK34	<i>mamK</i> _{AMB-1} [15]	this work	[3]
659	pEK35	<i>mamK</i> _{MS-1} [15]	this work	[4]
660	pEK36	<i>mamKshort</i> _{MSR-1} [16]	this work	[5]
661	pEK37	<i>mamK</i> _{AMB-1} [16]	this work	[6]
662	pEK40	<i>mamK</i> _{MSR-1} [16]	this work	[7]
663	pEK42	<i>egfp_LCLQGE_mamKshort</i> _{MSR-1} [14]	this work	[8]
664	pAS_K	<i>egfp_LCLQGE_mamK</i> _{MSR-1} [14]	(Scheffel, 2007)	[9]
665	pAS_K1	<i>mamK_GSI_egfp</i> [14]	this work	[10]
666	pAS_K2	<i>egfp_SAI_mamK</i> [14]	this work	[11]
667	pAS_J	<i>mamJ_egfp</i> [14]	(Scheffel <i>et al.</i> , 2006)	[12]
668	pK19 <i>mobGII</i>	-	(Katzen <i>et al.</i> , 1999)	[13]
669	pBBR1MCS-2	-	(Kovach <i>et al.</i> , 1994)	[14]
670	pBBRP <i>mamDC</i>	-	(Lang <i>et al.</i> , 2009)	[15]
671	pBBRP <i>mamAB</i>	-	(Lang <i>et al.</i> , 2009)	[16]
672	Primer	Sequence (5' - 3')	Restriction site	

673	EKmamK_F02	<u>CATATGTGGATTGATCTGTTAGC</u>	<i>NdeI</i>
674	EKmamK_R02	<u>GGATCCTCACTGACCGGAAAC</u>	<i>BamHI</i>
675	EKmamK_F_kurz	<u>CATATGAGTGAAGGTGAAGG</u>	<i>NdeI</i>
676	EKmamK_R02	<u>GGATCCTCACTGACCGGAAAC</u>	<i>BamHI</i>
677	EK_mamK_AMB1_F	<u>CATATGAGTGAAGGTGAAGGCC</u>	<i>NdeI</i>
678	EK_mamK_AMB1_R2	<u>GGATCCTCACGAGCCGGA</u>	<i>BamHI</i>
679	EK_mamK_MS1_F	<u>CATATGAGTGAAGGTGAAGGC</u>	<i>NdeI</i>
680	EK_mamK_MS1_R2	<u>GGATCCTCACGAGCCGGAG</u>	<i>BamHI</i>
681	EK2_K_u_f	<u>TCTAGAGTAGCCGGCCTCGCTCCTGGG</u>	<i>XbaI</i>
682	EK_K_u_r	<u>CCCGGGGATTGCTAACTAGTCAGGT</u>	<i>SmaI</i>
683		CTCTATTTATTCTTATCTTC	<i>SpeI</i>
684	EK_K_d_f	<u>ACTAGTCACGTCAAGGACCCGACTTTTG</u>	<i>SpeI</i>
685	EK2_K_d_r	<u>CCCGGG GGATCCATTTCCGCCTTCTTCCAGTC</u>	<i>BamHI</i>
686	ASEGFP_f10	<u>GAATTCATGGTGAGCAAGGGCGAG</u>	<i>BamHI</i>
687	ASEGFP_r11	CTCGCCCTGCAGGCACAGCTTGTACAGCTCGTCCAT	-
688	ASmamKs_f3	TGCCTGCAGGGCGAGCTGTGGATTGATCTGTTA	-
689	ASmamKe_r2	<u>TCTAGACTACTGACCGGAAACGTCACC</u>	<i>XbaI</i>
690	EK_K_f	TTGCTGCTCCCGCCGTTG	
691	EK_probeK02_r	TTGTCCAAGCCATAGCCG	
692	Name	Relevant genotype or phenotype	Construction
693	<i>Magnetospirillum</i>	MSR-1 E10, Δ <i>mamK</i> , Rif ^r ,	this work
694	<i>gryphiswaldense</i> ,		
695	Δ <i>mamK</i>	Strep ^r ,	
696	<i>Magnetospirillum</i>	Rif ^r , Strep ^r derivative of	(Schultheiss <i>et al.</i> , 2004)

697	<i>gryphiswaldense</i> MSR-1	DSM6361 (WT)	
698	<i>Magnetospirillum</i>	Rif ^r , Strep ^r , Δ <i>mamJ</i>	(Scheffel <i>et al.</i> , 2006)
699	<i>gryphiswaldense</i> MSR-1,		
700	Δ <i>mamJ</i>		
701	<i>Magnetospirillum</i>		
702	<i>gryphiswaldense</i> MSR-1B	Rif ^r , Strep ^r , spontaneous	
703		deletion mutant,	
704		lacking 40.4 kb within MAI,	
705		<i>mag</i> ⁻	
706			
707			(Schübbe <i>et al.</i> , 2003;
708			Ullrich <i>et al.</i> , 2005)
709			
710	<i>Magnetospirillum</i>	WT	(Kawaguchi <i>et al.</i> , 1992)
711	<i>magneticum</i> AMB-1	ATCC700264	
712			
713			
714	<i>E. coli</i> DH5 α	F ⁻ <i>supE44</i> DacU169	
715		(80/ <i>lacZ</i> Δ <i>lacU169</i> (Φ 80/ <i>lacZ</i> Δ M15)	
716		<i>hsdR17recA1endA1gyrA96thi-1relA1</i>	(Bethesda
717		Research Laboratories, 1986)	
718	<i>E. coli</i> BW29427	<i>thrB1004 pro thi rpsL hsdS lacZ</i> Δ M15	
719		RP4-1360 Δ (<i>araBAD</i>)567 Δ <i>dapA</i>	

720 1341::[*erm pir*(Wildtyp)]*tra* K.A.
721 Datsenko
722 and B.L.
723 Wanner
724 (Purdue
725 University,
726 IN, USA)
727
728
729
730
731
732
733
734
735
736
737
738
739
740
741
742
743

- 744 Adams, D. W. and Errington, J. (2009) Bacterial cell division: assembly, maintenance
745 and disassembly of the Z ring. *Nat Rev Microbiol* **7**: 642-653.
- 746 Balkwill, D., Maratea, D. and Blakemore, R. P. (1980) Ultrastructure of a magnetotactic
747 spirillum. *J Bacteriol* **141**: 1399-1408.
- 748 Bethesda Research Laboratories (1986) BRL pUC host: *E. coli* DH5 alpha competent
749 cells. *Focus* **8**: 1-19.
- 750 Blakemore, R., Maratea, D. and Wolfe, R. (1979) Isolation and pure culture of
751 freshwater magnetic spirillum in chemically defined medium. *J Bacteriol* **140**: 720-
752 729.
- 753 Briegel, A., Ortega, D. R., Tocheva, E. I., Wuichet, K., Li, Z., Chen, S., et al. (2009)
754 Universal architecture of bacterial chemoreceptor arrays. *Proc Natl Acad Sci USA*
755 **106**: 17181-17186.
- 756 Carballido-Lopez, R. (2006) The bacterial actin-like cytoskeleton. *Microbiol Mol Biol Rev*
757 **70**: 888-909.
- 758 Carballido-Lopez, R. and Errington, J. (2003) A dynamic bacterial cytoskeleton. *Trends*
759 *Cell Biol* **13**: 577-583.
- 760 Derman, A. I., Becker, E. C., Truong, B. D., Fujioka, A., Tucey, T. M., Erb, M. L., et al.
761 (2009) Phylogenetic analysis identifies many uncharacterized actin-like proteins
762 (Alps) in bacteria: regulated polymerization, dynamic instability and treadmilling in
763 Alp7A. *Mol Microbiol* **73**: 534-552.
- 764 Ding, Y., Li, J., Liu, J., Yang, J., Jiang, W., Tian, J., et al. (2009) Deletion of the *ftsZ*-like
765 gene results in the production of superparamagnetic magnetite magnetosomes in
766 *Magnetospirillum gryphiswaldense*. *J Bacteriol* **192**: 1097-1105.

- 767 Dye, N. A., Pincus, Z., Theriot, J. A., Shapiro, L. and Gitai, Z. (2005) Two independent
768 spiral structures control cell shape in *Caulobacter*. *Proc Natl Acad Sci USA* **102**:
769 18608-18613.
- 770 Faivre, D., Böttger, L. H., Matzanke, B. F. and Schüler, D. (2007) Intracellular magnetite
771 biomineralization in bacteria proceeds by a distinct pathway involving membrane-
772 bound ferritin and an iron(II) species. *Angew Chem Int Ed Engl* **46**: 8495-8499.
- 773 Frankel, R. and Bazylinski, D. (2006) How magnetotactic bacteria make magnetosomes
774 queue up. *Trends Microbiol* **14**: 329-331.
- 775 Gamba, P., Veening, J.-W., Saunders, N. J., Hamoen, L. W. and Daniel, R. A. (2009)
776 Two-step assembly dynamics of the *Bacillus subtilis* divisome. *J Bacteriol* **191**:
777 4186-4194.
- 778 Gorby, Y. A., Beveridge, T. J. and Blakemore, R. (1988) Characterization of the bacterial
779 magnetosome membrane. *J Bacteriol* **170**: 834-841.
- 780 Grünberg, K., Müller, E. C., Otto, A., Reszka, R. and Linder, D. (2004) Biochemical and
781 proteomic analysis of the magnetosome membrane in *Magnetospirillum*
782 *gryphiswaldense*. *Appl Environ Microbiol* **70**: 1040-1050.
- 783 Grünberg, K., Wawer, C., Tebo, B. M. and Schüler, D. (2001) A large gene cluster
784 encoding several magnetosome proteins is conserved in different species of
785 magnetotactic bacteria. *Appl Environ Microbiol* **67**: 4573-4582.
- 786 Ho, S., Hunt, H., Horton, R., Pullen, J. and Pease, L. (1989) Site-directed mutagenesis
787 by overlap extension using the polymerase chain reaction. *Gene* **77**: 51-59.
- 788 Jogler, C., Kube, M., Schübbe, S., Ullrich, S., Teeling, H., Bazylinski, D. A., et al.
789 (2009a) Comparative analysis of magnetosome gene clusters in magnetotactic

- 790 bacteria provides further evidence for horizontal gene transfer. *Environ Microbiol*
791 **11**: 1267-1277.
- 792 Jogler, C., Lin, W., Meyerdierks, A., Kube, M., Katzmann, E., Flies, C., et al. (2009b)
793 Toward cloning of the magnetotactic metagenome: identification of magnetosome
794 island gene clusters in uncultivated magnetotactic bacteria from different aquatic
795 sediments. *Appl Environ Microbiol* **75**: 3972-3979.
- 796 Jogler, C. and Schüler, D. (2007) Genetic analysis of magnetosome biomineralization.
797 In: Magnetoreception and magnetosomes in bacteria. D., S. (ed). Springer-Verlag
798 Berlin Heidelberg, pp. 133-161.
- 799 Jogler, C. and Schüler, D. (2009) Genomics, genetics, and cell biology of magnetosome
800 formation. *Annu Rev Microbiol* **63**: 501-521.
- 801 Jones, L. J., Carballido-Lopez, R. and Errington, J. (2001) Control of cell shape in
802 bacteria: helical, actin-like filaments in *Bacillus subtilis*. *Cell* **104**: 913-922.
- 803 Katzen, F., Becker, A., Ielmini, M. V., Oddo, C. G. and Ielpi, L. (1999) New mobilizable
804 vectors suitable for gene replacement in gram-negative bacteria and their use in
805 mapping of the 3' end of the *Xanthomonas campestris* pv. *campestris* gum
806 operon. *Appl Environ Microbiol* **65**: 278-282.
- 807 Kawaguchi, R., Burgess, J. and Matsunaga, T. (1992) Phylogeny and 16S rRNA
808 sequence of *Magnetospirillum* sp. AMB-1, an aerobic magnetic bacterium. *Nucl*
809 *Acids Res* **20**: 1140.
- 810 Kirschvink, J. L. (1982) Paleomagnetic evidence for fossil biogenic magnetite in western
811 Crete. *Earth Plan Sci Lett* **59**: 388-392.
- 812 Kobayashi, A., Kirschvink, J. L., Nash, C. Z., Kopp, R. E., Sauer, D. A., Bertani, L. E., et
813 al. (2006) Experimental observation of magnetosome chain collapse in

- 814 magnetotactic bacteria: sedimentological, paleomagnetic, and evolutionary
815 implications. *Earth Plan Sci Lett* **245**: 538-550.
- 816 Komeili, A. (2006) Cell biology of magnetosome formation. In: Magnetoreception and
817 magnetosomes in bacteria. Schüler, D. (ed). Springer-Verlag Berlin Heidelberg,
818 pp. 163-173.
- 819 Komeili, A. (2007) Molecular mechanisms of magnetosome formation. *Annu Rev*
820 *Biochem* **76**: 351-366.
- 821 Komeili, A., Li, Z., Newman, D. K. and Jensen, G. J. (2006) Magnetosomes are cell
822 membrane invaginations organized by the actin-like protein MamK. *Science* **311**:
823 242-245.
- 824 Komeili, A., Vali, H., Beveridge, T. J. and Newman, D. K. (2004) Magnetosome vesicles
825 are present before magnetite formation, and MamA is required for their activation.
826 *Proc Natl Acad Sci USA* **101**: 3839-3844.
- 827 Kovach, M. E., Phillips, R. W., Elzer, P. H., Roop, R. M. and Peterson, K. M. (1994)
828 pBBR1MCS: a broad-host-range cloning vector. *BioTechniques* **16**: 800-802.
- 829 Laemmli, U. K. (1970) Cleavage of structural proteins during the assembly of the head
830 of bacteriophage T4. *Nature* **227**: 680-685.
- 831 Lang, C., Pollithy, A. and Schüler, D. (2009) Identification of promoters for efficient gene
832 expression in *Magnetospirillum gryphiswaldense*. *Appl Environ Microbiol* **75**:
833 4206-4210.
- 834 Li, J. L., Pan, Y., Chen, G., Liu, Q., Tian, L. and Lin, W. (2009) Magnetite magnetosome
835 and fragmental chain formation of *Magnetospirillum magneticum* AMB-1:
836 transmission electron microscopy and magnetic observations. *Geophys J Int* **177**:
837 33-42.

- 838 Li, Z. and Jensen, G. (2009) Electron cryotomography: a new view into microbial
839 ultrastructure. *Curr Opin Microbiol* **12**: 1-8.
- 840 Li, Z., Trimble, M. J., Brun, Y. V. and Jensen, G. (2007) The structure of FtsZ filaments
841 in vivo suggests a force-generating role in cell division. *EMBO J* **26**: 4694-4708.
- 842 Lučić, V., Forster, F. and Baumeister, W. (2005) Structural studies by electron
843 tomography: from cells to molecules. *Annual Reviews of Biochemistry* **74**: 833-
844 865.
- 845 Marmur, J. (1961) A procedure for the isolation of deoxyribonucleic acid from
846 microorganisms. *J Mol Biol* **3**: 208-218.
- 847 Mastronarde, D. N. (2005) Automated electron microscope tomography using robust
848 prediction of specimen movements. *J Struct Biol* **152**: 36-51.
- 849 Milne, J. L. S. and Subramaniam, S. (2009) Cryo-electron tomography of bacteria:
850 progress, challenges and future prospects. *Nat Rev Microbiol* **7**: 666-675.
- 851 Møller-Jensen, J., Jensen, R. B., Löwe, J. and Gerdes, K. (2002) Prokaryotic DNA
852 segregation by an actin-like filament. *EMBO J* **21**: 3119-3127.
- 853 Murat, D., Quinlan, A., Vali, H. and Komeili, A. (2010) Comprehensive genetic dissection
854 of the magnetosome gene island reveals the step-wise assembly of a prokaryotic
855 organelle. *Proc Natl Acad Sci U S A* **107**: 5593-5598.
- 856 Nakazawa, H., Arakaki, A., Narita-Yamada, S., Yashiro, I., Jinno, K., Aoki, N., et al.
857 (2009) Whole genome sequence of *Desulfovibrio magneticus* strain RS-1
858 revealed common gene clusters in magnetotactic bacteria. *Genome Res* **19**:
859 1801-1808.

- 860 Nickell, S., Forster, F., Linaroudis, A., Net, W. D., Beck, F., Hegerl, R., et al. (2005) TOM
861 software toolbox: acquisition and analysis for electron tomography. *J Struct Biol*
862 **149**: 227-234.
- 863 Ohuchi, S. and Schüler, D. (2009) *In vivo* display of a multisubunit enzyme complex on
864 biogenic magnetic nanoparticles. *Appl Environ Microbiol* **75**: 7734-7738.
- 865 Pradel, N., Santini, C., Bernadac, A., Fukumori, Y. and Wu, L. (2006) Biogenesis of
866 actin-like bacterial cytoskeletal filaments destined for positioning prokaryotic
867 magnetic organelles. *Proc Natl Acad Sci USA* **103**: 17485-17489.
- 868 Pradel, N., Santini, C., Bernadac, A., Shih, Y., Goldberg, M. and Wu, L. (2007) Polar
869 positional information in *Escherichia coli* spherical cells. *Biochem Biophys Res Co*
870 **353**: 493-500.
- 871 Richter, M., Kube, M., Bazylinski, D. A., Lombardot, T., Glöckner, F. O., Reinhardt, R.
872 and Schüler, D. (2007) Comparative genome analysis of four magnetotactic
873 bacteria reveals a complex set of group-specific genes implicated in
874 magnetosome biomineralization and function. *J Bacteriol* **189**: 4899-4910.
- 875 Rioux, J.-B., Philippe, N., Pereira, S., Pignol, D., Wu, L.-F. and Ginet, N. (2010) A
876 second actin-like MamK protein in *Magnetospirillum magneticum* AMB-1 encoded
877 outside the genomic magnetosome island. *PLoS ONE* **5**: e9151.
- 878 Salje, J. and Löwe, J. (2008) Bacterial actin: architecture of the ParMRC plasmid DNA
879 partitioning complex. *EMBO J* **27**: 2230-2238.
- 880 Sambrook, J. and Russel, D. (2001) *Molecular cloning: a laboratory manual.*, p. 999.
881 Cold Spring Harbor Laboratory Press.

- 882 Scheffel, A. (2007) Molekulare und strukturelle Untersuchung zur Bildung von
883 Magnetosomen und zur Assemblierung von Magnetosomenketten. *Doctoral*
884 *thesis*. 1-194.
- 885 Scheffel, A., Gruska, M., Faivre, D., Linaroudis, A., Graumann, P. L., Plitzko, J. and
886 Schüler, D. (2006) An acidic protein aligns magnetosomes along a filamentous
887 structure in magnetotactic bacteria. *Nature* **440**: 110-114.
- 888 Scheffel, A. and Schüler, D. (2007) The acidic repetitive domain of the *Magnetospirillum*
889 *gryphiswaldense* MamJ protein displays hypervariability but is not required for
890 magnetosome chain assembly. *J Bacteriol* **189**: 6437-6446.
- 891 Schübbe, S. (2005) Untersuchung zur molekularen Regulation und Organisation der
892 *mam*-Gene in *Magnetospirillum gryphiswaldense* MSR-1. *Doctoral thesis*. 1-167.
- 893 Schübbe, S., Kube, M., Scheffel, A., Wawer, C., Heyen, U., Meyerdierks, A., et al.
894 (2003) Characterization of a spontaneous nonmagnetic mutant of
895 *Magnetospirillum gryphiswaldense* reveals a large deletion comprising a putative
896 magnetosome island. *J Bacteriol* **185**: 5779-5790.
- 897 Schübbe, S., Würdemann, C., Peplies, J., Heyen, U., Wawer, C., Glöckner, F. O. and
898 Schüler, D. (2006) Transcriptional organization and regulation of magnetosome
899 operons in *Magnetospirillum gryphiswaldense*. *Appl Environ Microbiol* **72**: 5757-
900 5765.
- 901 Schüler, D. (2004a) Characterization of the magnetosome membrane in
902 *Magnetospirillum gryphiswaldense*. In: Biominerlization. Baeuerlein, E. (ed).
903 Wiley-VCH Verlag GmbH, pp. 109-118.

- 904 Schüler, D. (2004b) Molecular analysis of a subcellular compartment: The
905 magnetosome membrane in *Magnetospirillum gryphiswaldense*. *Arch Microbiol*
906 **181**: 1-7.
- 907 Schüler, D. (2008) Genetics and cell biology of magnetosome formation in
908 magnetotactic bacteria. *FEMS Microbiol Rev* **32**: 654-672.
- 909 Schüler, D. and Köhler, M. (1992) The isolation of a new magnetic spirillum. *Zentralbl*
910 *Mikrobiol* **147**: 150-151.
- 911 Schultheiss, D., Kube, M. and Schüler, D. (2004) Inactivation of the flagellin gene *flaA* in
912 *Magnetospirillum gryphiswaldense* results in nonmagnetotactic mutants lacking
913 flagellar filaments. *Appl Environ Microbiol* **70**: 3624-3631.
- 914 Schultheiss, D. and Schüler, D. (2003) Development of a genetic system for
915 *Magnetospirillum gryphiswaldense*. *Arch Microbiol* **179**: 89-94.
- 916 Simpson, E. T. (2008) Electron holography of isolated and interacting magnetic
917 nanocrystals. *Doctoral thesis*. 1-197.
- 918 Taoka, A., Asada, R., Sasaki, H., Anzawa, K., Wu, L. and Fukumori, Y. (2006) Spatial
919 localizations of Mam22 and Mam12 in the magnetosomes of *Magnetospirillum*
920 *magnetotacticum*. *J Bacteriol* **188**: 3805-3812.
- 921 Taoka, A., Asada, R., Wu, L. and Fukumori, Y. (2007) Polymerization of the actin-like
922 protein MamK, which is associated with magnetosomes. *J Bacteriol* **189**: 8737-
923 8740.
- 924 Ullrich, S., Kube, M., Schübbe, S., Reinhardt, R. and Schüler, D. (2005) A hypervariable
925 130-kilobase genomic region of *Magnetospirillum gryphiswaldense* comprises a
926 magnetosome island which undergoes frequent rearrangements during stationary
927 growth. *J Bacteriol* **187**: 7176-7184.

928 Vats, P., Shih, Y.-L. and Rothfield, L. (2009) Assembly of the MreB-associated
929 cytoskeletal ring of *Escherichia coli*. *Mol Microbiol* **72**: 170-182.

930

931

For Peer Review

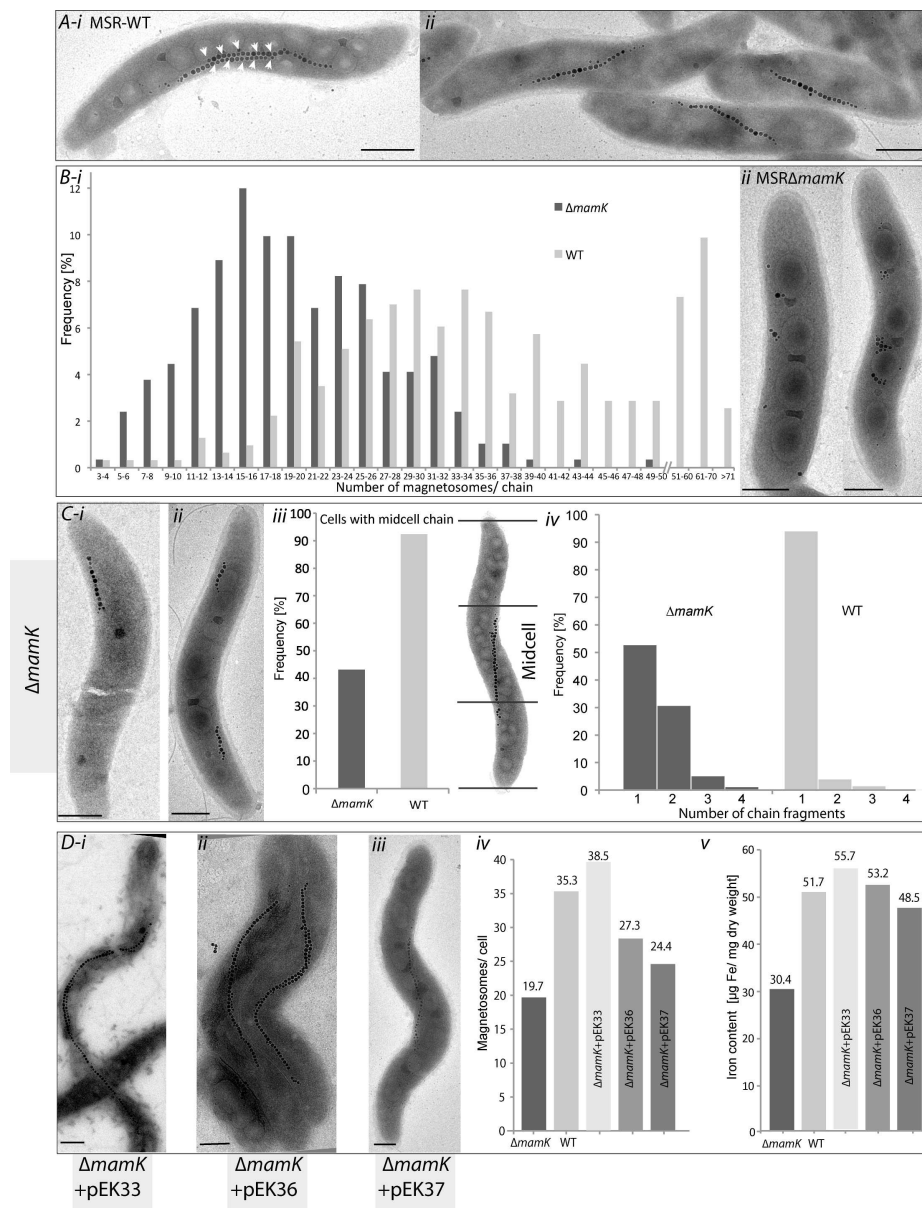


Fig. 1: Overview of morphologies and magnetosome chain organizations found in MSRΔmamK cells and WT. (A-i-ii) TEM micrographs of MSR WT cells. White arrows indicate parallel chains. (B-i) Statistical analysis of magnetosome particles per chain and micrographs of MSRΔmamK cells displaying dispersed magnetosomes (B-ii). (C-i-ii) Micrographs of MSRΔmamK cells displaying ectopic chain localization, and statistical analysis of chain position (C-iii), and chain numbers (C-iv) in MSRΔmamK. (D-i-iii) TEM micrographs of transcomplemented MSRΔmamK cells with various plasmids. Magnetosome numbers and iron contents of the strains are shown in (D-v). Scale bars 500 nm.

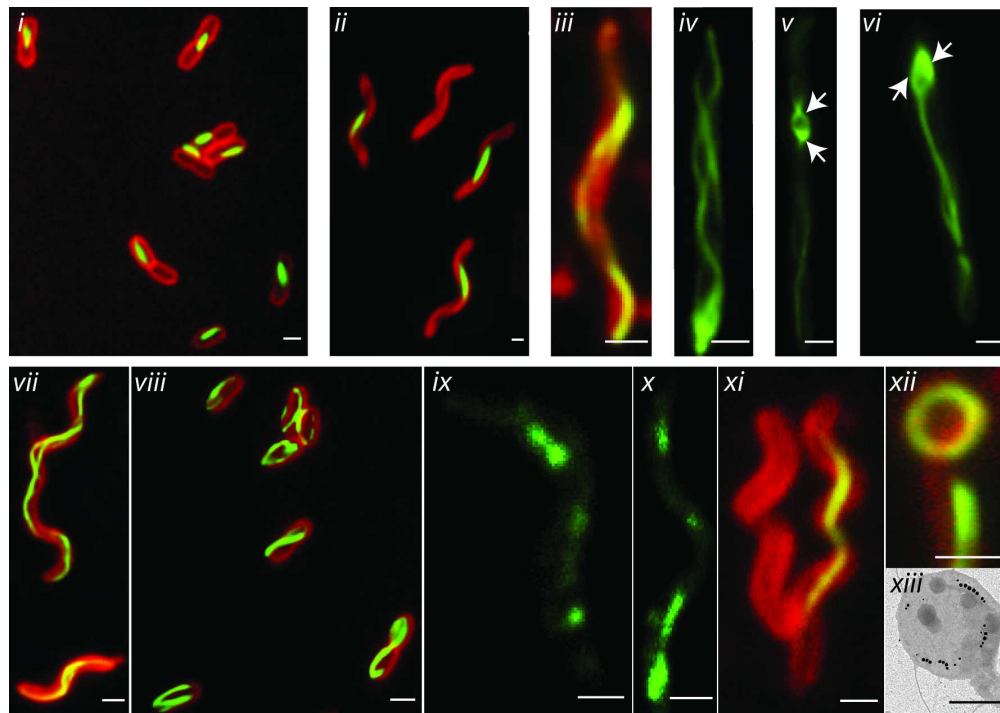


Fig. 2: Fluorescence micrographs of *E. coli*, MSR (and MSR-1B) and AMB expressing different EGFP fusions. (i) Overlay of FM4-64 (red) and *egfp* (green) recombinant *E. coli* expressing pAS_K1. Localization pattern of MamK_GSI_eGFP. (ii) pAS_K1 expressed in non-magnetic mutant MSR-1B. (iii) MSR WT expressing pAS_K. (iv - vi) MSR Δ *mamK* mutant of MSR-1 expressing pAS_K (eGFP_LCLQGE_MamK) resulting in loop-shaped or spiral localization patterns. Loop-like structures are observed at midcell (white arrows). (vii) pAS_K expressed in MSR-1B exhibiting helical filaments. (viii) Overlay of FM4-64 and *egfp* image of recombinant *E. coli* expressing pAS_K. Helical filaments are visible. (ix - x) MSR Δ *mamK* mutant expressing eGFP fused MamJ (pAS_J). (xi) Overlay of FM4-64 and *egfp* of AMB WT expressing pAS_K resulting in a long filamentous localization throughout the entire cell. (xii) MSR Δ *mamK* mutant expressing pAS_K in MSR Δ *mamK* in a spheroplast cell. (xiii) TEM micrograph of a spheroplast cell. Scale bars 500 nm. 150x106mm (300 x 300 DPI)

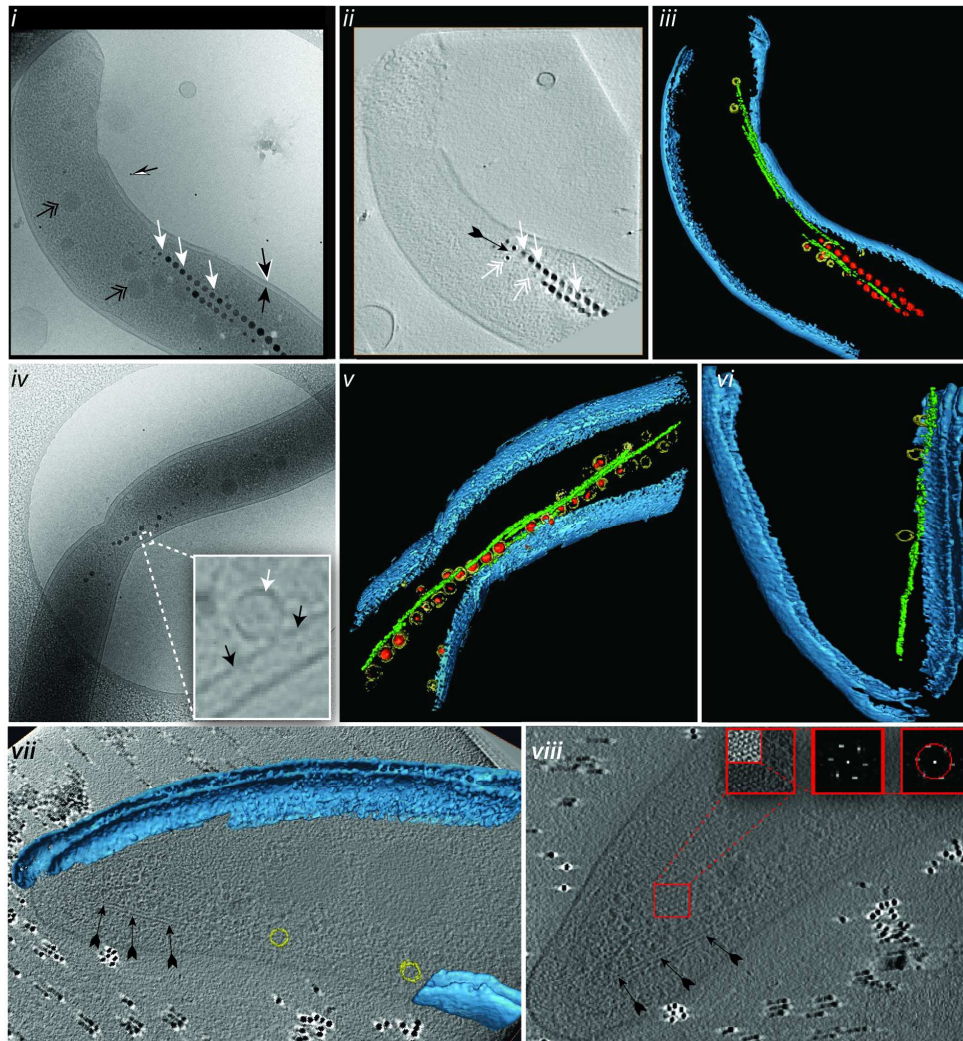


Fig. 3: Cryo-electron micrographs and tomograms of MSR WT. (i) Cryo-electron micrograph of a WT cell after the acquisition of a tilt series in vitrified ice. (ii) x-y slice of a tomogram from (i). (iii) Surface rendered volume of the WT cell. Depicted are the cell membrane (blue), magnetite crystals (red), vesicles (yellow) and filaments (green). (iv) Cryo-electron micrograph of WT cell in early division state after acquisition of a tilt series. Inset *iv*: MM vesicle from *iv* invaginating from the CM (black arrows CM, white arrow MM). (v) Surface rendered volume of cell shown in (iv). (vi) Surface rendered pole of MSR WT cell exhibiting filaments close to the pole membrane. (vii-viii) x-y slices of WT tomogram (vi). (Insets of *viii*): power spectra of a putative chemoreceptor array, lattice distance 10.5 nm. Arrow tips; black: CM and black with white rim OM, black-white: fiducial gold marker (15nm), white: magnetite crystals, double-white (*ii*): vesicle membrane, black with flething: filament, double-black: PHB granules.

165x172mm (300 x 300 DPI)

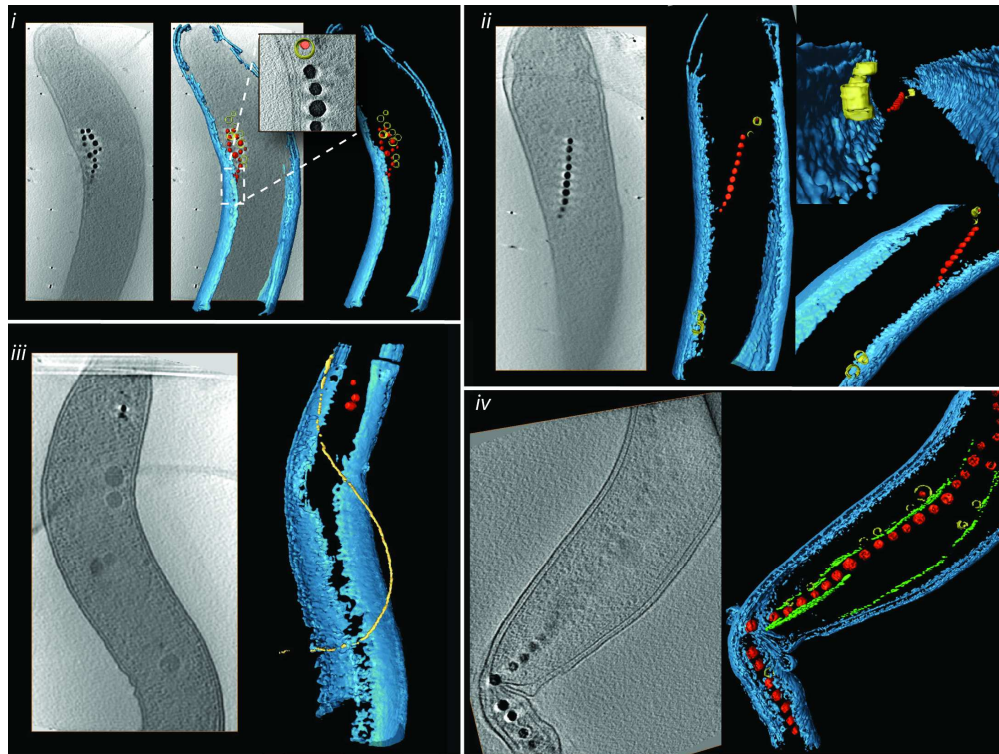


Fig. 4: (i-iv) Cryo-electron tomograms of $MSR\Delta mamK$ in early stationary phase grown under standard conditions (30°C, FSM medium), flagella (yellow) in (iii). (iv) transcomplemented $MSR\Delta mamK$ mutant in late division state expressing *mamK* from pEK42. Surface-rendered representation of a segment of the cells showing vesicles (yellow) and magnetite crystals (red). Different three-dimensional orientations show the variety of the pleiotropic phenotypes (membrane in blue) of $MSR\Delta mamK$ mutants. The apparent absence of MM (vesicles, yellow) from mature magnetite crystals (red) is due to the adverse effect of variable diffraction contrast during tilting as a result of the crystalline magnetite.

184x138mm (300 x 300 DPI)



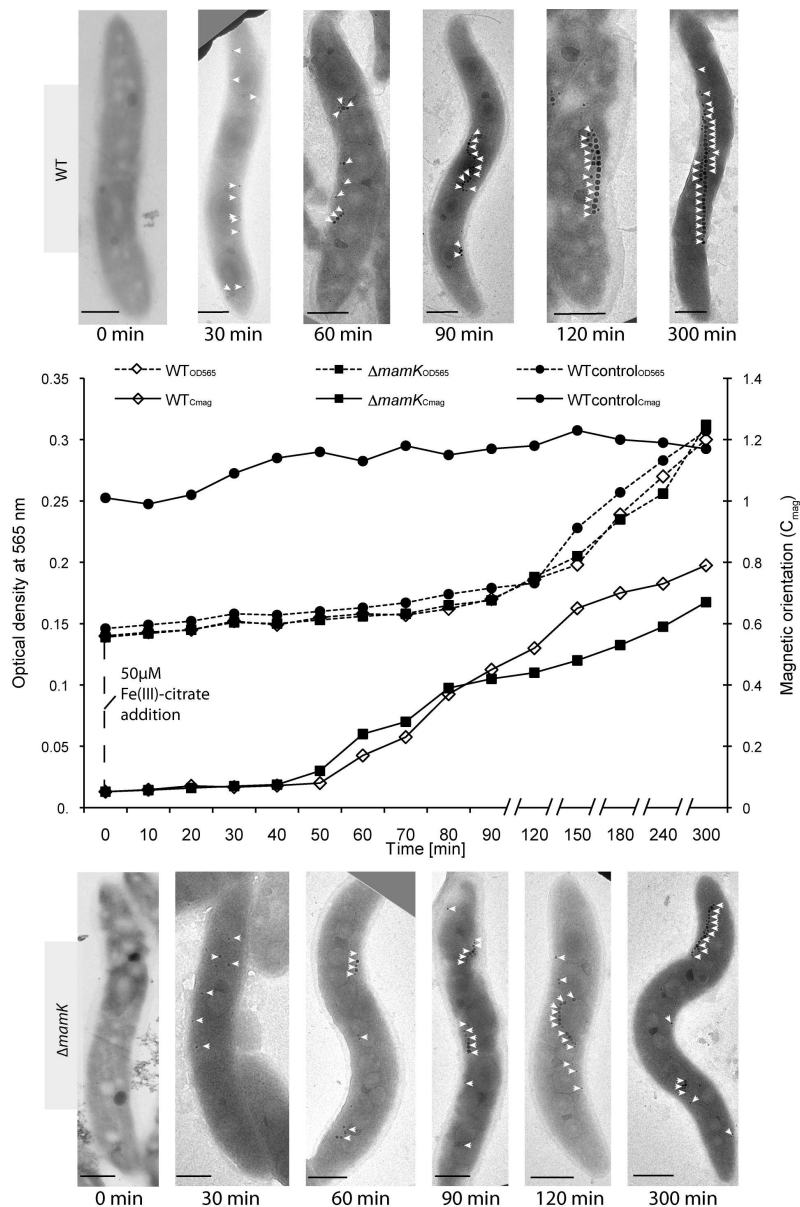


Fig. 5: Time course of magnetosome synthesis and chain assembly after iron induction in *M. gryphiswaldense* WT and MSR $\Delta mamK$. Non-magnetic cells were cultured for 300 min in LIM. 50 μM Fe(III)-citrate was added at 0 min and growth (dashed line) was analyzed by optical density at 565 nm. WT_{control} cells were cultured under standard un-induced growth conditions in 50 μM Fe(III)-citrate FSM medium. Solid lines: magnetic orientation (C_{mag}). Electron micrographs of cells from aliquots taken at various time points are shown. Scale bars 500 nm.